Excited states of ribosome translocation revealed through integrative molecular modeling

Paul C. Whitford[a], Aqeel Ahmed[b], Yanan Yu[c], Scott P. Hennelly[a], Florence Tama[b], Christian M. T. Spahn[d], José N. Onuchic[e,1], and Karissa Y. Sanbonmatsu[1,a]

[a]Theoretical Biology and Biophysics Group, Theoretical Division, Los Alamos National Laboratory, Los Alamos, NM 87545; [b]Department of Chemistry and Biochemistry, University of Arizona, 1041 East Lowell Street, Tucson, AZ 85721; [c]Department of Computer Science, Florida State University, Tallahassee, FL 32306; [d]Institut fur Medizinische Physik und Biophysik, Charite—Universitatsmedizin Berlin, Ziegelstrasse 5–9, 10117-Berlin, Germany; and [e]Center for Theoretical Biological Physics and Department of Physics, Rice University, 6100 Main, Houston, TX 77005-1827

Contributed by José N. Onuchic, May 26, 2011 (sent for review March 16, 2011)

The dynamic nature of biomolecules leads to significant challenges when characterizing the structural properties associated with function. While X-ray crystallography and imaging techniques (such as cryo-electron microscopy) can reveal the structural details of stable molecular complexes, strategies must be developed to characterize configurations that exhibit only marginal stability (such as intermediates) or configurations that do not correspond to minima on the energy landscape (such as transition-state ensembles). Here, we present a methodology (MDfit) that utilizes molecular dynamics simulations to generate configurations of excited states that are consistent with available biophysical and biochemical measurements. To demonstrate the approach, we present a sequence of configurations that are suggested to be associated with transfer RNA (tRNA) movement through the ribosome (translocation). The models were constructed by combining information from X-ray crystallography, cryo-electron microscopy, and biochemical data. These models provide a structural framework for translocation that may be further investigated experimentally and theoretically to determine the precise energetic character of each configuration and the transition dynamics between them.

free-energy landscape | modeling transient configurations | molecular machine | tRNA hybrid | translation

Structural biology techniques, including X-ray crystallography and cryo-electron microscopy (cryo-EM), have provided extraordinary insights into the details of the functional configurations of biomolecular machines, such as the ribosome (1–11). These successes have relied on the ability to isolate structurally homogeneous populations of the molecular complexes. Molecular systems undergo continual fluctuations (12). However, when the energetic minimum associated with a particular configuration is sufficiently deep, the structural fluctuations only lead to minor deviations from the average. The structural models provided by these approaches describe the average coordinates inside each basin, and occasionally the structural distribution within a basin may also be characterized (13–16). When the energy landscape contains multiple basins of comparable free energy, one must "trap" the system (5) in a particular configuration, which results in a modified energy landscape (17). This is often true for X-ray crystallographic models, because scattering patterns may only be obtained if the molecules in the crystal are of sufficiently similar configuration and orientation. In this respect, cryo-EM is more flexible because heterogeneities (i.e., molecules that are not trapped in the desired basin) may be computationally removed after data collection (8, 11). These sorting methods allow one to access information about less populated basins of attraction. The smaller number of images in these basins may result in limited resolution; however, several recent studies with $\approx 10^6$ images have produced reconstructions of subpopulations with subnanometer resolution. In principle, it may be possible to obtain cryo-EM reconstructions of configurations within the transition-state ensemble (TSE), though the population in the TSE is proportional to $e^{-\Delta G_{\mathrm{TSE}}\beta}$, where ΔG_{TSE} is the barrier height. Therefore, for barriers greater than 1–2 $k_\beta T$, less than 10% of the images will be of molecules in the TSE, which makes direct observation with cryo-EM impractical.

Due to the transient nature of biomolecular dynamics (12) and the marginal stability exhibited by many functional configurations (18), structural insights into large-scale rearrangements of molecular machines is rarely direct. For example, imaging is often impeded by the fact that large-scale movements must not be associated with deep energetic minima (or, conversely, large barriers), or else the time scales of the processes would rapidly exceed biological time scales. To illustrate this point, consider diffusion of transfer RNA (tRNA) inside of the ribosome. In the context of tRNA accommodation, it was shown through explicit-solvent simulations (3.2 million atoms for 2.1 μs) (19) that the free-energy barriers associated with large-scale movements of tRNA inside the ribosome are approximately 5–10 $k_B T$. Because tRNA molecules traverse large length scales (>100 Å), low barriers implicate broad basins of attraction, which make it difficult to populate structurally homogeneous ensembles.

The dynamic nature of biomolecular function is highlighted by the ribosome: a massive (>2 MDa) molecular complex that undergoes a variety of conformational rearrangements during the elongation cycle of protein synthesis. It is generally described as being composed of two subunits, the 30S ("small") and 50S ("large") subunits. Both subunits have an A, P, and E site, and tRNA molecules simultaneously associate with a site on each subunit (20). During peptide-bond formation the nascent chain's covalent bond with the P-site tRNA is broken and a new bond is formed with the aminoacylated-tRNA (aa-tRNA), which results in partial displacement of the A-site tRNA in the direction of the P site (21–23). Following peptide-bond formation, the tRNA molecules move (along with the mRNA) by one binding site inside the ribosome.* This movement is collectively referred to as "translocation," and it results in a vacant A site, which enables reading of the next codon in the mRNA. Chemical probing data first revealed that tRNA molecules adopt "hybrid" configurations during translocation (24), where a single tRNA is associated with the P site of the small subunit and the E site of the large subunit to form the P/E configuration. The second tRNA also enters hybrid configurations, where it bridges the A site of the small subunit and P site of the large subunit to transiently form A/P* and A/P

Author contributions: P.C.W., F.T., C.M.T.S., J.N.O., and K.Y.S. designed research; P.C.W., A.A., Y.Y., and K.Y.S. performed research; P.C.W., S.P.H., and K.Y.S. analyzed data; and P.C.W., S.P.H., F.T., J.N.O., and K.Y.S. wrote the paper.

The authors declare no conflict of interest.

Data deposition: The structural models are available at the Sanbonmatsu team's web page (http://www.t6.lanl.gov/kys/).

*The P-site tRNA moves to the E site and the A-site tRNA to the P site.

[1]To whom correspondence may be addressed. E-mail: kys@lanl.gov or jonuchic@ucsd.edu.

This article contains supporting information online at www.pnas.org/lookup/suppl/doi:10.1073/pnas.1108363108/-/DCSupplemental.

configurations (23, 24). This movement is accelerated by EF-G, a five-domain GTPase that is transiently associated with the ribosome during translocation. While the ribosome is a well-characterized molecular machines (25–27), with the aforementioned energy landscape considerations, probing the structural aspects of the ribosome during function has proven to be quite challenging.

Since the first crystallographic structures of the ribosome were obtained 10 years ago (1, 2, 6, 28, 29), many efforts have aimed to uncover the structural details of ribosomal translocation. Currently, there are crystal structures of ribosomes in hybrid-like configurations without tRNA molecules bound (3, 4), ribosomes with classically bound tRNAs in the A and P sites without EF-G (the pretranslocation complex) (30, 31), or with classical tRNAs in the P and E sites and EF-G absent (15) or bound (the post-translocation complex) (5). For the transiently populated hybrid configurations, cryo-EM has provided electron density reconstructions for ribosomes with EF-G and a single tRNA in P/E configurations(pp/E,pe/E) (8, 32) and also ribosomes with two hybrid tRNAs in the absence of EF-G (33, 34). Finally, a recent crystallographic model was obtained with a single tRNA in a hybrid P/E configuration (35). Cryo-EM techniques have also been used to describe the structural aspects of reverse translocation (36). Because reverse translocation occurs in the absence of EF-G and on time scales of minutes (in contrast to EF-G-accelerated forward translocation, which occurs on microsecond to millisecond time scales). Here, even though the reaction rate was decreased significantly, the intermediates remained inaccessible. Observed conformational changes and tRNA movements are likely due to spontaneous intersubunit rotation and tRNA hybrid state formation, which occur within the pretranslocational complex on the sub-second time scale (26). Because EF-G-accelerated forward translocation is the biologically relevant process, characterizing its structural and energetic details represents a long-standing objective for the ribosome field. Despite many advances, an atomic model of a ribosome with two tRNAs in hybrid configurations and EF-G associated has yet to be obtained through conventional experimental techniques alone.

With the transient properties of molecular motions, and the important and widespread roles that these rearrangements play in cellular function, strategies must be developed that can afford a more complete understanding of the atomic details of these processes. Here, we demonstrate how a computational approach (MDfit) may be used to incorporate information from X-ray crystallography, cryo-EM, and biochemical measurements to suggest the structural details of excited-state configurations of the ribosome during translocation. These models are stereochemically correct, are consistent with experimental knowledge, and are devoid of atomic clashes. We illustrate the utility of this framework by producing atomic models of the ribosome during translocation with two tRNA molecules in hybrid configurations and EF-G associated. While these models are consistent with existing knowledge, further experimental data may be incorporated, in order to refine the descriptions of these states. Through iterative model building and experimentation, consensus models may be obtained and used to guide antibiotic design.

Results and Discussion

MDfit. We use a simulation-based approach (MDfit, see *SI Methods*) to obtain all-atom models for configurations of macromolecular complexes for which there is a cryo-electron microscopy density available and a crystallographic (or NMR) structure of an alternate configuration. Specifically, we employ all-atom structure-based models (SBM) (37, 38) with an additional potential energy contribution that introduces a basin of attraction about the EM density (39)[†]. Grounded in the energy landscape theory of biomolecular dynamics (40), structure-based models define the "native" configuration as the global energetic minimum, and they can accurately describe the local fluctuations of biomolecular complexes (37, 38, 41–46). Fluctuations about a particular basin (i.e., "excited" configurations) often correlate with biologically relevant rearrangements (46–49), allowing these simple models to have built-in information about these functionally relevant excited (transiently forming) states (Fig. 1, dashed red lines). These forcefields have also provided insights into the structural composition of transition-state ensembles, which can include cracking (partial unfolding and refolding of substructures) (41, 43, 47, 50) and other disorder-to-order transitions, as seen in the 3′-CCA end of aa-tRNA during accommodation (38). With the reduced computational cost of these models (in comparison to explicit-solvent simulations), when using these forcefields as the foundation for modeling excited configurations and transition-state ensembles it is possible to perform more extensive searches of the accessible phase space. The significant increase in accessible sampling is highlighted by a recent study in which we used SBMs to simulate the ribosome and spontaneous aa-tRNA accommodation events were observable (38) without the use of enhanced sampling methods. Additionally, fitting a large system, such as the ribosome, can be performed with a single desktop computer. By increasing the sampled space, this approach has the potential to identify complex rearrangements that are associated with transient configurations of the ribosome and other molecular machines.

When using SBMs to identify excited states, one simply needs to "capture" the excited configurations that agree with the target restraints. In our simplest implementation, the target restraint is based solely on a cryo-EM electron density map (see *SI Text*). To account for this information, we introduce an energetic term

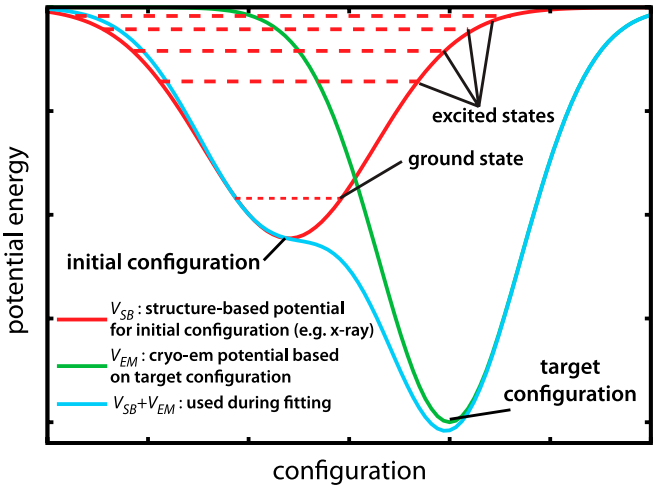

Fig. 1. Schematic representation of a potential energy surface for which excited states and transiently populated configurations are accessible. When constructing atomic models from cryo-EM using MDfit, one starts with a potential energy function based on the initial configuration (red). A structure-based model (SBM) for the initial configuration encodes that configuration as the global energetic minimum. The local fluctuations in SBMs often correlate with functional motions, allowing excited/transient configurations to be more accessible than nonphysiological configurations, such as globally denatured configurations. In explicit-solvent models, the excited configurations may be orthogonal to the functional displacements, which can lead to artifacts in the modeled configurations. To populate the excited configurations of the original model (dashed red lines), we introduce an energetic weight based on knowledge of the target (e.g., from cryo-EM) complex (green). The sum of the terms yields a downhill energy profile (blue), where the target configuration corresponds to the global minimum. To obtain structural models of the ribosome in intermediate configurations of translocation, we define a starting potential energy function based on a classical ribosome configuration and the biasing term is based on cryo-EM reconstructions of hybrid configurations.

[†]Structure-based models are available through the smog@ctbp web server (http://smog.ucsd.edu) and the EM-fitting source code is also available at http://mdfit.lanl.gov.

(Fig. 1, green) that is based on the correlation between the experimental electron density and the theoretical electron density (which is calculated for the simulated conformations as a function of time). Because the structure-based model lacks energetic roughness, the sum of the two energetic terms results in a "downhill" energy profile (Fig. 1, blue) and the target structure resides within the new global minimum (when the EM term is sufficiently strong). We then integrate the equations of motion until the maximum in the correlation between the experimental and simulated densities is reached.

It should be stressed that the effectiveness of this approach is due to the underlying potential energy function (i.e., the structure-based potential). Specifically, in SBMs the excited states are correlated with functional molecular displacements (46–49). With other potential energy functions, such as explicit-solvent models, the lowest-energy excited configurations do not necessarily correspond to functionally relevant motions. For example, in explicit-solvent simulations of the ribosome, if the employed ion model does not adequately screen the negatively charged backbone phosphate atoms in RNA, then the system may unfold, rather than find a biologically relevant excited configuration. This point is evident in studies where explicit-solvent simulations are used for cryo-EM modeling. In those studies, many additional restraints must be included during fitting (such as secondary structure restraints) to prevent such effects (51, 52). These secondary structure restraints are not based on predictions, or energetic considerations, but are determined from the starting configuration. By including restraints based on the initial configuration, the explicit-solvent forcefields are forced to mimic structure-based forcefields, where the initial configuration is defined as the global energetic minimum. By introducing a sufficient number of restraints on the system, those approaches only allow for a few preassigned fluctuations to occur, whereas these fluctuations are intrinsic in the SBMs.

To demonstrate the ability of MDfit to produce atomic models that are consistent with cryo-EM densities, we performed fitting for a test of proteins and compared the performance of MDfit to several other flexible-fitting protocols. The test set proteins all have multiple crystallographic structures available in the Protein Data Bank. For each protein, we generated a theoretical EM density for one configuration (i.e., the target configuration) and then initiated fitting from the alternate structure. With few exceptions, MDfit performed as well as the other three methods (see *SI Text* for details), as measured by the rmsd from the target configuration and the correlation between the theoretical density of the fitted structure and the target configuration.

Obtaining Atomic Models of Hybrid Configurations. To demonstrate how the MDfit methodology may be used to determine atomic models of large-scale systems for which only electron microscopy data is available, we employed this technique using a crystal structure of a classical ribosome as the initial model and a target P/E hybrid configuration that was identified through cryo-EM experiments (8) (Fig. 2). Consistent with the EM construct, the model employed only included one tRNA molecule. The initial model has a tRNA in the P/P configuration (Fig. 3*C*, transparent red). Prior to fitting,[‡] the molecular complex was manually aligned as a rigid-body to the density map. After fitting, the configuration agrees well with the EM density, and the vast majority of the atomic model lies inside the high density regions of the EM map (Fig. 3*A*). In addition to an approximately 45 Å displacement of the 3′-CCA end during fitting (Fig. 3*C* and Movie S1), the 30S subunit also performed ratchet-like (53) rotation.

[‡]In this manuscript, "fitting" refers to the process of energy minimization and/or simulation with a potential energy function that includes EM and/or biochemical contributions. The fitting simulations are performed until the structure converges around the lowest-energy configuration.

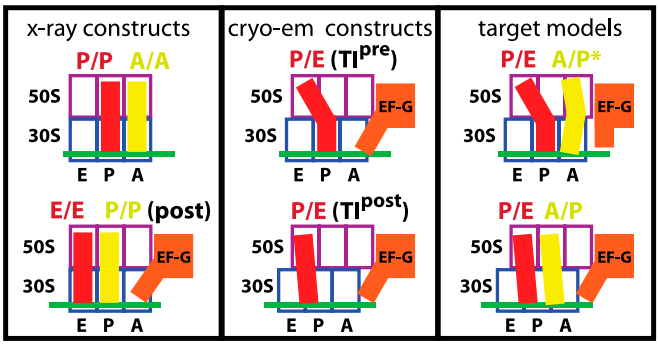

Fig. 2. Summary of available experimental constructs and target models of transient configurations that are associated with translocation in the ribosome. (*Left*) Crystal structures are available for the ribosome with classical tRNAs in pretranslocation configurations without EF-G (top) (30, 31), a post-translocation configuration with EF-G (bottom) (5) and with a single hybrid tRNA (35) (not shown). (*Center*) Cryo-EM has provided densities of ribosomes with a single tRNA and EF-G in intermediate configurations associated with translocation (TI^{pre}, TI^{post}) (8). (*Right*) The target models represent translocation in vivo: two tRNAs and EF-G engaged in forward translocation. While direct characterization of these configurations has been elusive, thus far, models may be obtained that are consistent with current knowledge. Such models can represent working atomic models that may be further refined through MDfit-like approaches. When sufficient restraints overconstrain the models, consensus may be reached.

The initial energy function has a global basin of attraction centered about the classical configuration, and only interactions that could not be satisfied in the target configuration were disrupted. By construction, the structure-based model assigns 1 unit of stabilizing energy per atom (37, 38). In preliminary fits, if the strength of the EM map was significantly larger (×10) than the assigned stabilizing energy, the secondary structure of the tRNA would locally melt, whereas when these terms were comparable the secondary structure remained formed during fitting. As noted earlier, with simulation-based fitting methods that employ explicit-solvent simulations, additional restraints are often included to prevent such effects (51, 52). In structure-based models, the secondary structure defined by the X-ray structure is encoded in the energetic basin. Because we employed an SBM, the reduced computational cost enabled the simulation of longer effective time scales, allowing for local melting to be reversible on computational time scales. Further, in the SBM, the classical secondary structure is energetically favored over denatured configurations. In contrast, with some explicit-solvent models the native secondary structure is not always stable, even for sequences that are known to be stable experimentally (54, 55). Thus, when using an explicit-solvent model, disrupted secondary structure can result, even though the secondary structure may be fully consistent with the EM density.

While local melting during fitting may resemble biomolecular cracking (41, 43, 47), the dynamics observed during the fitting process should not be interpreted as reflecting the dynamics in solution. At first glance, this may appear inconsistent with the claim that these models implicitly carry information of the excited configurations. To be clear, the structure-based potential energy function has the excited configurations encoded in it. Though, during fitting a strong additional potential energy term is introduced in order to populate the configurations that are consistent with the EM density. This secondary energetic contribution does not have any information, either explicit or implicit, about the dynamics of reaching the excited configuration, and it can therefore result in high-energy transition routes. With SBMs, if high-energy routes are sampled during the fit, the longer accessible time scales allow the system to relax to a low-energy conformation on computationally accessible time scales.

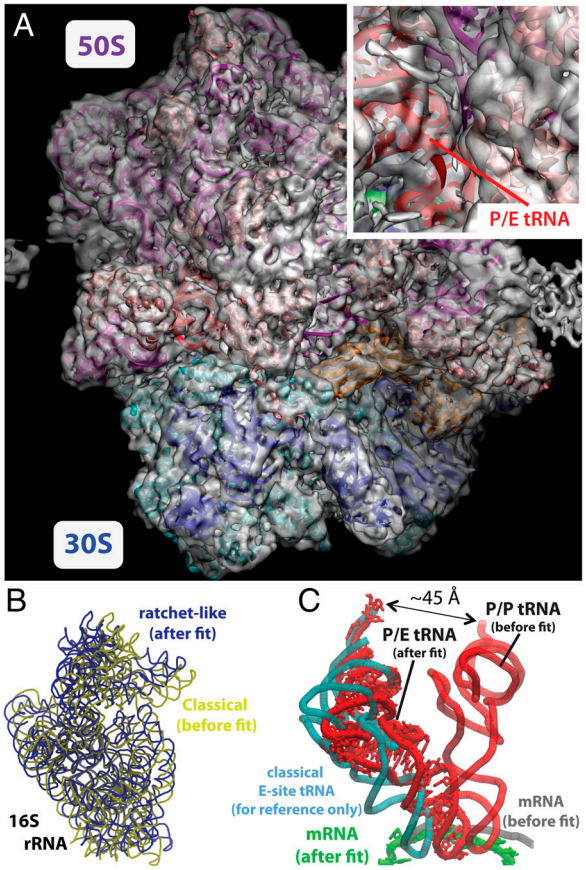

Fig. 3. Hybrid configuration with one tRNA obtained with MDfit. Adopting a hybrid configuration of the ribosome involves large-scale conformational rearrangements. (*A*) Cryo-EM density (gray) of a hybrid P/E configuration with a fitted atomic model (PDB ID codes 2XSY, 2XTG) (8). (*Inset*) The P/E tRNA (red) fits well inside of the experimental density. (*B*) 16S rRNA before (yellow) and after (blue) fitting (alignment based on the 23S rRNA coordinates). Fitting involves a large-scale rotation of the 30S subunit (which is composed of 16S rRNA and proteins. 52,172 atoms). (*C*) In the starting model, the tRNA molecule is in the P/P configuration (red tubes). During the fitting process, the tRNA adopts a P/E configuration (45 Å red with side chains shown) and the 3′-CCA end aligns well with the configuration of an E/E tRNA (blue tubes, shown for reference). E/E tRNA was not included during fitting. A shift in the mRNA position is concomitant with rotation of the 30S.

Atomic Models of Hybrid Configurations with Two tRNAs and EF-G. There are no high-resolution electron density maps or crystallographic models available for the ribosome during intermediate stages of translocation with two fully resolved tRNAs and EF-G, which is the biologically relevant complex. Therefore, we had to extend the MDfit method to account for the inherent differences between the target model (hybrid configurations with two tRNAs and EF-G) and the available reconstructions (hybrid configuration with one tRNA and EF-G. Fig. 2). The A-site tRNA is not present in the EM constructs. Accordingly, we did not fit it to the density and we maintained its association by introducing restraints with the A-site tRNA and the ribosome (See *SI Text*), which were based on biochemical observations that implicate distinct hybrid-configured tRNAs (23, 24). Specifically, chemical probing data indicates that following peptide-bond formation, a single tRNA bridges the 30S A(P) site and 50S P(E) site, forming A/P (P/E) configuration (24). Additionally, prior to EF-G catalyzed translocation of the mRNA, the system is not puromycin reactive, indicating that the A-site tRNA is only partially associated with the P site of the 50S, suggesting occupation of an A/P* configuration (where the CCA end of the A-site tRNA is partially translocated) (56).

To identify which configurations of the A-site tRNA (A/P* and A/P) are consistent with specific arrangements of the P-site tRNA, the 30S and 50S subunits and EF-G during translocation, we prepared several models that include different combinations of A-site tRNA configurations and EM densities (see *SI Text*). Specifically, we employed the MDfit method to produce models for all combinations of densities (TI^{pre} and TI^{post}) and A-site tRNA configurations (A/A,A/P*,A/P). Introducing these independent restraints into the forcefield can result in large-scale distortions if the combination of A-site tRNA and density is not consistent. When the restraints are not mutually consistent, distortions in the atomic models may be introduced. In most cases, such distortions are visible to the eye, and those combinations may be discarded immediately (see *SI Text* for full analysis). Here, we will focus our discussion on the configurations that are devoid of such distortions. While we classify the models as likely and less-likely, based on visible distortions, additional biochemical/biophysical measurements will be necessary to delineate the energetic balance between them.

An atomic model of the A/P*-P/E configuration (Fig. 4, *Top*) was prepared by fitting all atoms in the system to an electron density of the TI^{pre} configuration (8), except for the A-site tRNA (it is not present in the EM reconstruction) and domain IV of EF-G (its density overlaps with the 30S A site; see *SI Text*). In the TI^{pre} map, the P/E tRNA configuration is accompanied by rotation of the 30S subunit, relative to the 50S subunit (Fig. 3*B*), and the mRNA is displaced with the 30S subunit. By construction, the structure-based forcefield includes stabilizing interactions between the classical A/A tRNA and the ribosome. To build models with the A-site tRNA in A/P* and A/P configurations, atomic restraints were introduced with the P site of the 50S rRNA. The A/P* configuration was most consistent with the TI^{pre} configuration of the ribosome (see *SI Text*). After fitting, the P/E tRNA overlaps well with the high density regions of the map, and all of EF-G is accommodated by its binding region on the ribosome except for domain IV (*SI Text*). While we normally consider distortions as a sign of an inconsistent set of structural restraints, rearrangements in domain IV of EF-G are consistent with other experimental reports. Specifically, smFRET measurements have demonstrated that EF-G associates with the ribosome prior to formation of the A/P-P/E conformation (58). Our model is consistent with this finding and suggests that EF-G likely undergoes a rearrangement in domain IV during this process. The orientation of domain IV in the A/P*-P/E model also suggests the molecular origin of EF-G's perturbative effects on the conformation/dynamics of protein S4 during initial association (23) (*SI Text*). Further, these models indicate that domain IV rearrangements may represent experimentally implicated movement of EF-G associated with translocation (23).

With the mRNA occupying its classical position on the 30S, it is not possible to fit domain IV into its density with a tRNA in the A/P* configuration. It is important to emphasize that we do not claim this model represents a stable configuration of the ribosome. Rather, it represents an atomic configuration that is consistent with independent pieces of information (puromycin reactivity measurements and the cryo-EM density), and it may be that it is only transiently formed.

Using the A/P*-P/E model as an initial configuration, we next fit the system to an electron density map of the TI^{post} configuration (8).[§] In this map, the mRNA is displaced by a distance of approximately one codon in length (3 nucleotides) and the 30S head undergoes a swivel-like rotation of approximately 15°. This swivel-like motion of the head allows the tRNA anticodon stem loop to simultaneously interact with two binding sites on the 30S subunit. That is, the codon that is in the P site when in the

[§]The A/P*-P/E model was used as the initial configuration, while the original structure-based forcefield (based on the A/A-P/P configuration) was employed.

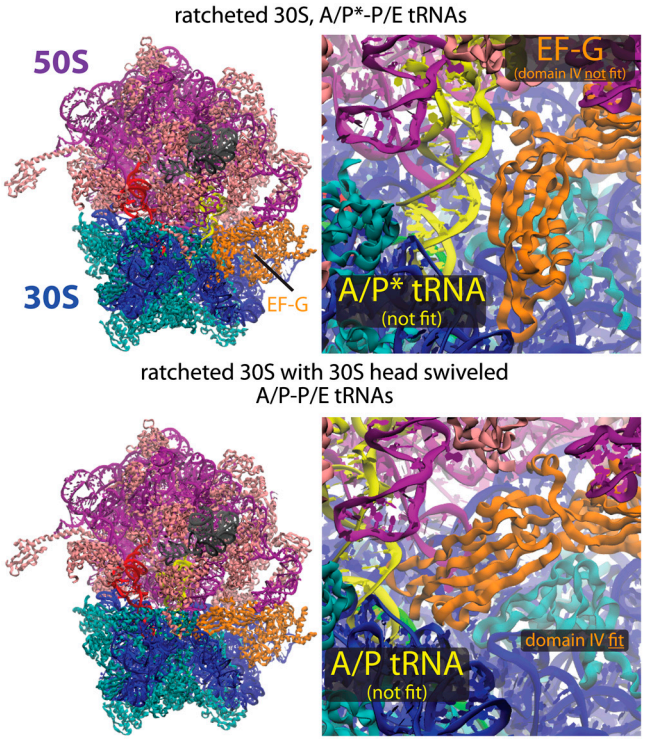

Fig. 4. Suggested models for transient configurations during translocation. (*Top Left*) Atomic model of the ribosome with tRNA molecules in a A/P*-P/E configuration, fitted to a cryo-EM density where the mRNA has not translocated (TI^{pre} configuration) (8). The A-site tRNA and domain IV of EF-G are not fit to the density. In the cryo-EM construct domain IV can enter the A site because there is no A/A tRNA present. Here, domain IV is not fit, but it is allowed to relax into an accessible low-energy configuration (top, right). (*Bottom*) Atomic model of the ribosome and tRNAs in an A/P-P/E configuration, fitted to a density map in which the mRNA has partially translocated (TI^{post}). The concomitant displacement of the A-site tRNA and partial mRNA translocation leads to available space for fitting domain IV of EF-G. Therefore, all atoms were fit to the density, except for the A/P tRNA. Model with densities shown are provided in the *SI Text*.

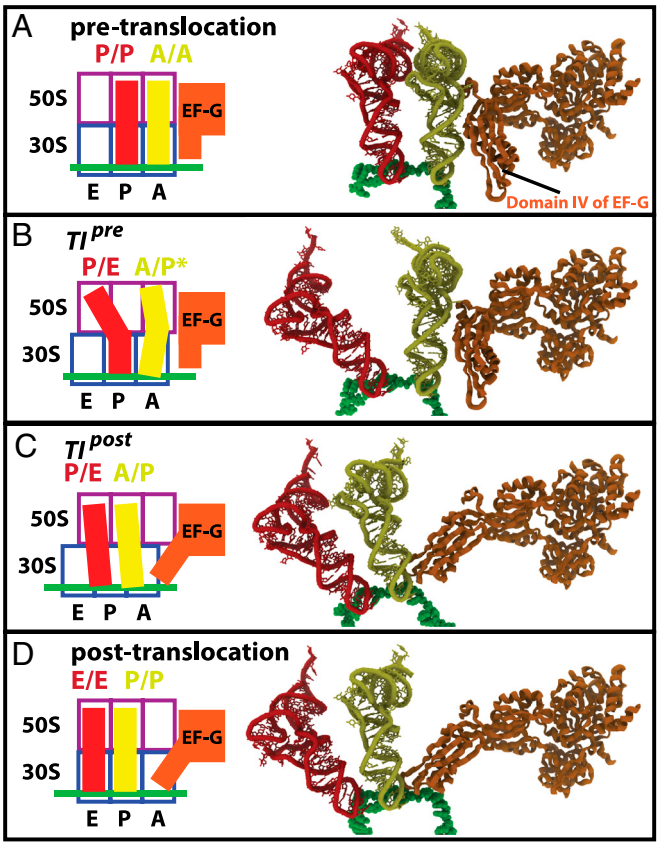

Fig. 5. Suggested models of tRNA molecules and EF-G during translocation. tRNA molecules move from (*A*) a classical A/A-P/P configuration, to hybrid (*B*) A/P*-P/E and (*C*) A/P-P/E configurations, and then to (*D*) a classical P/P-E/E configuration. While the precise timing of EF-G association during translocation is intensely debated, if association with the ribosome occurs prior to the tRNAs reaching a A/P-P/E configuration, these models suggest that it would likely enter an energetically strained configuration (*A* and *B*). Such an accumulation and release of strain suggests an active role of domain IV during mRNA translocation, which is consistent with the detrimental effect of domain IV deletion on mRNA translocation (23).

A/A-P/P conformation is displaced and it contacts residues in both the P site and E site of the 30S subunit [referred to as the pe/E configuration; see Ratje et al. (8) for a detailed discussion on intrasubunit binding events]. This partial translocation of the mRNA led to the observation that this configuration (pe/E) of the ribosome, tRNA, and EF-G may be consistent with an additional tRNA occupying the biochemically implicated A/P configuration (23, 24). To explore this notion, we introduced restraints between the A-site tRNA and 50S P site, which induced movement of the tRNA from the A/P* to A/P configuration (see *SI Methods*). We find that when the A-site tRNA adopts an A/P configuration, it is possible to also include the EM contribution of domain IV of EF-G during fitting. That is, the A-site tRNA anticodon stem loop fits in A site of the 30S, while domain IV of EF-G is fit into its EM density. Alternate conformations of the A-site tRNA and ribosome resulted in distortions of the tRNA (*SI Text*), suggesting that the pe/E conformation is most consistent with the A/P tRNA (Fig. 4).

Conclusions

Not only do the dynamics of molecular machines span many length scales, but the time scales of individual rearrangements are often rapid (milliseconds), which indicates the underlying energy landscapes are not composed of deep minima. Rather, molecular complexes continuously interconvert between energetic basins that are separated by a continuum of TSEs and excited states. To fully characterize the gamut of accessible configurations of these systems, it is necessary to develop tools that utilize information from structural techniques (providing information about minima), biochemical data (59–61) that can provide information about the TSEs and excited states and bioinformatic analyses (62) that can provide signatures of complex dynamics. Simulation-based modeling approaches are an ideal integration point where information from these complementary experimental techniques may be simultaneously used to provide a more complete picture of biomolecular dynamics. As examples, integrative modeling (63) studies have incorporated experimental information to determine the global arrangement of a nuclear pore complex (64) and genomic data to identify functional configurations of a two-component signal transduction systems (65), while other simulation-based methods have used SAXS data to provided in-solution ensemble descriptions of protein kinases (66, 67). The work presented here shows how one may incorporate data from X-ray crystallography, cryo-EM, and biochemical measurements to suggest atomic details of the elusive configurations associated with tRNA translocation in the ribosome (Fig. 5). As additional experimental information becomes available, simulation-based approaches may be used to resolve the atomic details of ribosomes in alternate stages of translation, ribosomes that are subject to different cellular stresses (such as elevated ion concentrations, change in temperatures, etc.) and ribosomes from higher-level organisms. Additionally, as distance measurements from single-molecule FRET become more precise (26, 27, 57), this information may also be introduced as restraints during modeling. By iteratively performing experiments and refin-

ing working models for complex biomolecular rearrangements, consensus models may be obtained that provide an unambiguous description of intermediates and transition-state ensembles associated with functional rearrangements.

ACKNOWLEDGMENTS. This work was supported by the Los Alamos National Laboratory (LANL) Laboratory Directed Research and Development program and National Institutes of Health Grant R01-GM072686. Work at the Center for Theoretical Biological Physics is sponsored by the National Science Foundation (NSF) (Grant PHY-0822283) and by NSF-MCB-1051438, and C.M.T.S. is supported by funding from Deutsche Forschungsgemeinschaft DFG (SFB 740 TP A3 and TP Z1, SP 1130/2-1). Additional funding was provided by NSF grant NSF-MCB-0744732. We are also grateful for computing time on the New Mexico Computing Applications Center Encanto Supercomputer. P.C.W. is funded by a LANL Director's Postdoctoral Fellowship.

1. Schluenzen F, et al. (2000) Structure of functionally activated small ribosomal subunit at 3.3 angstrom resolution. *Cell* 102:615–623.
2. Yusupov MM, et al. (2001) Crystal structure of the ribosome at 5.5 a resolution. *Science* 292:883–296.
3. Ben-Shem A, Jenner L, Yusupova G, Yusupov M (2010) Crystal structure of the eukaryotic ribosome. *Science* 330:1203–1209.
4. Zhang W, Dunkle JA, Cate JHD (2009) Structures of the ribosome in intermediate states of ratcheting. *Science* 325:1014–1017.
5. Gao Y-G, et al. (2009) The structure of the ribosome with elongation factor g trapped in the posttranslocational state. *Science* 326:694–699.
6. Ban N, Nissen P, Hansen J, Moore PB, Steitz TA (2000) The complete atomic structure of the large ribosomal subunit at 2.4 angstrom resolution. *Science* 289:905–920.
7. Frank J, Spahn CMT (2006) The ribosome and the mechanism of protein synthesis. *Rep Prog Phys* 69:1383–1417.
8. Ratje AH, et al. (2010) Head swivel on the ribosome facilitates translocation by means of intra-subunit tRNA hybrid sites. *Nature* 468:713–716.
9. Spahn CMT, et al. (2001) Structure of the 80s ribosome from saccharomyces cerevisiae-tRNA-ribosome and subunit-subunit interactions. *Cell* 107:373–386.
10. Armache JP, et al. (2010) Cryo-EM structure and rRNA model of a translating eukaryotic 80s ribosome at 5.5-a resolution. *Proc Natl Acad Sci USA* 107:19748–19753.
11. Mulder AM, et al. (2010) Visualizing ribosome biogenesis: Parallel assembly pathways for the 30s subunit. *Science* 330:673–677.
12. Frauenfelder H, Sligar SG, Wolynes PG (1991) The energy landscapes and motions of proteins. *Science* 254:1598–1603.
13. García AE, Krumhansl JA, Frauenfelder H (1997) Variations on a theme by debye and waller: From simple crystals to proteins. *Proteins* 29:153–160.
14. García AE (1992) Large-amplitude nonlinear motions in proteins. *Phys Rev Lett* 68:2696–2699.
15. Korostelev A, Trakhanov S, Laurberg M, Noller HF (2006) Crystal structure of a 70s ribosome-tRNA complex reveals functional interactions and rearrangements. *Cell* 126:1065–77.
16. Vaiana AC, Sanbonmatsu KY (2009) Stochastic Gating and Drug-Ribosome Interactions. *J Mol Biol* 386:648–661.
17. Whitford PC, et al. (2011) *Ribosomes: Structure, Function and Dynamics* (Springer, New York), pp 303–319.
18. Munro J, Sanbonmatsu KY, Spahn CMT, Blanchard SC (2009) Navigating the ribosome's metastable energy landscape. *Trends Biochem Sci* 34:390–400.
19. Whitford PC, Onuchic JN, Sanbonmatsu KY (2010) Connecting energy landscapes with experimental rates for aminoacyl-tRNA accommodation in the ribosome. *J Am Chem Soc* 132:13170–13171.
20. Demeshkina N, Jenner LB, Yusupova G, Yusupov MM (2010) Interactions of the ribosome with mrna and trna. *Curr Opin Struct Biol* 20:325–332.
21. Yonath A (2005) Ribosomal crystallography: Peptide bond formation, chaperone assistance and antibiotic activity. *Mol Cells* 20:1–16.
22. Gindulyte A, et al. (2006) The transition state for formation of the peptide bond in the ribosome. *Proc Natl Acad Sci USA* 103:13327–13332.
23. Rodnina MV, Savelsbergh A, Wintermeyer W (1999) Dynamics of translation on the ribosome: Molecular mechanics of translocation. *FEMS Microbiol Rev* 23:317–333.
24. Moazed D, Noller HF (1989) Intermediate states in the movement of transfer RNA in the ribosome. *Nature* 342:142–148.
25. Marshall RA, Aitken CE, Dorywalska M, Puglisi JD (2008) Translation at the single-molecule level. *Annu Rev Biochem* 77:177–203.
26. Blanchard SC (2009) Single-molecule observations of ribosome function. *Curr Opin Struct Biol* 19:103–109.
27. Petrov A, et al. (2011) Dynamics of the translational machinery. *Curr Opin Struct Biol* 21:137–145.
28. Harms J, et al. (2001) High resolution structure of the large ribosomal subunit from a mesophilic Eubacterium. *Cell* 107:679–688.
29. Wimberly BT, et al. (2000) Structure of the 30s ribosomal subunit. *Nature* 407:327–339.
30. Jenner LB, Demeshkina N, Yusupova G, Yusupov MM (2010) Structural aspects of messenger RNA reading frame maintenance by the ribosome. *Nat Struct Mol Biol* 17:555–560.
31. Voorhees RM, Weixlbaumer A, Loakes D, Kelley AC, Ramakrishnan V (2009) Insights into substrate stabilization from snapshots of the peptidyl transferase center of the intact 70s ribosome. *Nat Struct Mol Biol* 16:528–533.
32. Frank J, Gao H, Sengupta J, Gao N, Taylor DJ (2007) The process of mRNA-tRNA translocation. *Proc Natl Acad Sci USA* 104:19671–19678.
33. Agirrezabala X, et al. (2008) Visualization of the hybrid state of tRNA binding promoted by spontaneous ratcheting of the ribosome. *Mol Cell* 32:190–197.
34. Julian P, et al. (2008) Structure of ratcheted ribosomes with tRNAs in hybrid states. *Proc Natl Acad Sci USA* 105:16924–16927.
35. Dunkle JA, et al. (2011) Structures of the bacterial ribosome in classical and hybrid states of tRNA binding. *Science* 332:981–984.
36. Fischer N, Konevega AL, Wintermeyer W, Rodnina MV, Stark H (2010) Ribosome dynamics and tRNA movement by time-resolved electron cryomicroscopy. *Nature* 466:329–333.
37. Whitford PC, et al. (2009) An all-atom structure-based potential for proteins: Bridging minimal models with all-atom empirical forcefields. *Proteins* 75:430–441.
38. Whitford PC, et al. (2010) Accommodation of aminoacyl-trna into the ribosome involves reversible excursions along multiple pathways. *RNA* 16:1196–1204.
39. Orzechowski M, Tama F (2008) Flexible fitting of high-resolution X-ray structures into cryo electron microscopy maps using biased molecular dynamics simulations. *Biophys J* 95:5692–5705.
40. Bryngelson JD, Onuchic JN, Socci ND, Wolynes PG (1995) Funnels, pathways, and the energy landscape of protein-folding—a synthesis. *Proteins* 21:167–195.
41. Whitford PC, Miyashita O, Levy Y, Onuchic JN (2007) Conformational transitions of adenylate kinase: Switching by cracking. *J Mol Biol* 366:1661–1671.
42. Roy M, et al. (2005) The native energy landscape for interleukin-1 beta. Modulation of the population ensemble through native-state topology. *J Mol Biol* 348:335–347.
43. Hyeon C, Jennings PA, Adams JA, Onuchic JN (2009) Ligand-induced global transitions in the catalytic domain of protein kinase A. *Proc Natl Acad Sci USA* 106:3023–3028.
44. Tama F, Valle M, Frank J, Brooks CL, III (2003) Dynamic reorganization of the functionally active ribosome explored by normal mode analysis and cryo-electron microscopy. *Proc Natl Acad Sci USA* 100:9319–9323.
45. Chennubhotla C, Rader AJ, Yang LW, Bahar I (2005) Elastic network models for understanding biomolecular machinery: from enzymes to supramolecular assemblies. *Phys Biol* 2:S173–180.
46. Wang Y, Rader AJ, Bahar I, Jernigan RL (2004) Global ribosome motions revealed with elastic network model. *J Struct Biol* 147:302–314.
47. Miyashita O, Onuchic JN, Wolynes PG (2003) Nonlinear elasticity, proteinquakes, and the energy landscapes of functional transitions in proteins. *Proc Natl Acad Sci USA* 100:12570–12575.
48. Korostelev A, Noller HF (2007) Analysis of structural dynamics in the ribosome by tls crystallographic refinement. *J Mol Biol* 373:1058–1070.
49. Kumar S, Ma B, Tsai C-J, Wolfson H, Nussinov R (1999) Folding funnels and conformational transitions via hinge-bending motions. *Cell Biochem Biophys* 31:141–164.
50. Olsson U, Wolf-Watz M (2010) Overlap between folding and functional energy landscapes for adenylate kinase conformational change. *Nat Commun* 1:111.
51. Trabuco LG, et al. (2011) Applications of the molecular dynamics flexible fitting method using molecular dynamics. *J Struct Biol* 173:420–427.
52. Villa E, et al. (2009) Ribosome-induced changes in elongation factor tu conformation control gtp hydrolysis. *Proc Natl Acad Sci USA* 106:1063–1068.
53. Frank J, Agrawal RK (2000) A ratchet-like inter-subunit reorganization of the ribosome during translocation. *Nature* 406:318–322.
54. Deng N-J, Cieplak P (2010) Free energy profile of RNA hairpins: A molecular dynamics simulation study. *Biophys J* 98:627–636.
55. Trabuco LG, et al. (2010) The role of L1 stalk-tRNA interaction in the ribosome elongation cycle. *J Mol Biol* 402:741–760.
56. Munro JB, et al. (2010) Spontaneous formation of the unlocked state of the ribosome is a multistep process. *Proc Natl Acad Sci USA* 107:709–714.
57. Ermolenko DN, et al. (2007) The antibiotic viomycin traps the ribosome in an intermediate state of translocation. *Nat Struct Mol Biol* 14:493–497.
58. Munro JB, et al. (2010) Correlated conformational events in EF-G and the ribosome regulate translocation. *Nat Struct Mol Biol* 17:1470–1477.
59. Dinman JD (2009) The eukaryotic ribosome: Current status and challenges. *J Biol Chem* 284:11761–11765.
60. Petrov AN, Meskauskas A, Roshwalb SC, Dinman JD (2008) Yeast ribosomal protein l10 helps coordinate tRNA movement through the large subunit. *Nucleic Acids Res* 36:6187–98.
61. Ramu P, et al. (2011) Nascent Peptide in the ribosome exit tunnel affects functional properties of the a-site of the peptidyl transferase center. *Mol Cell* 41:321–330.
62. Alexander RW, Eargle J, Luthey-Schulten Z (2010) Experimental and computational determination of tRNA dynamics. *FEBS Lett* 584:376–386.
63. Webb B, et al. (2011) Modeling of proteins and their assemblies with the integrative modeling platform. *Methods Mol Biol* 781:377–397.
64. Alber F, et al. (2007) The molecular architecture of the nuclear pore complex. *Nature* 450:695–701.
65. Schug A, Weigt M, Onuchic JN, Hwa T, Szurmant H (2009) High-resolution protein complexes from integrating genomic information with molecular simulation. *Proc Natl Acad Sci USA* 106:22124–22129.
66. Jamros MA, et al. (2010) Proteins at work: A combined small angle X-ray scattering and theoretical determination of the multiple structures involved on the protein kinase functional landscape. *J Biol Chem* 285:36121–36128.
67. Yang S, Blachowicz L, Makowski L, Roux B (2010) Multidomain assembled states of hck tyrosine kinase in solution. *Proc Natl Acad Sci USA* 107:15757–15762.